

Role of Spatial Curvature in a Dark Energy Interacting Model

Trupti Patil* and Sukanta Panda †

*† Department of Physics, Indian Institute of Science Education and Research Bhopal,
Bhopal - 462066, India

Abstract

This paper investigates the effects of spatial curvature in a model where dark matter and dark energy interact. The analysis employs a range of datasets, including CMB, BAO, Type Ia Supernova, $H(z)$ from cosmic chronometers, H_0 measurements from Megamasers and SH0ES, growth rate data and strong lensing time delay measurements, to assess the model's fit and explore the late-time dynamics of the interacting dark sector in a non-flat cosmological framework. The study indicates that introducing curvature does affect the Hubble constant (H_0) and the structure growth parameter (S_8), and also helps in alleviating the tensions between early and late universe observations to some extent. The observational data shows an indication for an open universe. This implies that the presence of curvature and its influence on Universe's evolution cannot be neglected entirely.

1 INTRODUCTION

Understanding the intricate balance of energy forms throughout the vast expanse of the universe, as well as characterizing their perturbations, are primary goals of both ongoing and forthcoming cosmological observations of the Cosmic Microwave Background (CMB) and the Large-Scale Structure (LSS) of the cosmos. A robustly supported perspective in cosmology is the adoption of the standard flat Λ CDM cosmological model, which is backed by extensive observational data. This is often based on the findings of numerous studies that use data from sources such as the Cosmic Microwave Background (CMB), Baryon Acoustic Oscillations (BAOs) and Type Ia supernovae (SNe-Ia) to constrain various cosmological parameters, including the curvature density parameter Ω_k (see, for instance, *Refs. [1–12]). The majority of these studies have shown that a flat universe is consistent with cosmological observations. However, recent observational probes [13–22] that attract considerable attention for the possibility of non-zero Ω_k values, which can influence the cosmic energy budget, add intrigue to this complex landscape. Also, there are well-studied curvature models motivated by string theory constructions, recently proposed in [23, 24] and investigated through observations in [25]. In this study, we further explore the possibility of non-zero spatial curvature.

Planck CMB power spectra, when analysed with the *Plik* likelihood, prefers a closed Universe $\Omega_k < 0$ at $\sim 3\sigma$ level ($\Omega_k = -0.044^{+0.018}_{-0.015}$). Whereas the joint constraint with BAO measurements shows a preference for a flat universe with $\Omega_k = -0.001 \pm 0.002$ [26], indicating a discrepancy in Ω_k , between CMB and BAO measurements. When the *Planck* temperature and polarization data are combined with the lensing reconstruction, yield fits consistent with flatness to within $\sim 1\%$ ($\Omega_k = -0.0106 \pm 0.0065$). These constraints with BAO data addition, yield $\Omega_k = -0.0007 \pm 0.0019$

*trupti19@iiserb.ac.in

†sukanta@iiserb.ac.in

*In Ref. 1, the authors conclude $|\Omega_k| < 0.0094$ (95% confidence) by combining data from the WMAP experiment and other sources. They remark that “a small deviation from flatness is expected and is worthy of future searches.”

[26,27], corresponding to a 1σ detection of flatness at an accuracy of 0.2%. As an independent probe of cosmic curvature, a recent BAO compilation from the recent extended Baryon Oscillation Spectroscopic Survey (eBOSS) [28] found Ω_k to be $0.078_{-0.099}^{+0.086}$. Additionally, an indication for a closed spatial curvature is also present in BAO data, using Effective Field Theories of LSS (EFTofLSS) [29], once the assumptions of flatness are removed from the beginning. These inconsistencies in the data for Ω_k constraints themselves give rise to what can be referred to as the curvature tension, as mentioned in [13]. Also, in [13, 14, 30, 31], they provide evidence for the possible discord among early and late universe observational probes (including BAO, Supernovae, lensing, and cosmic shear measurements) in Λ CDM models which permit curvature. These findings challenged the spatial flatness assumptions present in the standard Λ CDM model and sparked a debate about the possibility of a small but non-zero spatial curvature in our universe. Notably, observations consistent with near-flat geometry cannot conclusively establish that the universe is spatially flat [32] unless supported by strong theoretical reasoning. Furthermore, incorrectly assuming a flat geometry for a spatially curved universe could significantly impact the inferred values of cosmological parameters [33]. Since allowing for spatial curvature can impact parameter constraints [33], it is essential to consider the curvature parameter and allow the observational data to determine the most likely scenario, avoiding possible biases introduced by the flatness assumption.

Furthermore, the authors of [14, 34–37] have found that the spatial curvature may significantly influence tension in the Hubble expansion parameter, H_0 , known as the Hubble tension, as well as the tension in the structure growth parameter, S_8 , referred to as the S_8 tension. In [36, 38–40] it is shown that though the impact of curvature is small, it does alter the H_0 and S_8 constraints when compared to results assuming flat spatial geometry. In [41], the authors presented that emerging spatial curvature carries the potential to resolve the Hubble constant tension[†] between high-redshift (CMB) and low-redshift (distance ladder) measurements, as shown using generated mock supernovae data. Therefore, in this manuscript, we aim to investigate this possibility of additional spatial curvature in the universe and its implications on H_0 and S_8 tensions. In particular, we intend to study the impact on the value of the Hubble constant and the existing more than 5σ tension between *Planck* CMB(2018) + Λ CDM estimate [26] and the SHOES [42] measurement, together with the $\sim 3\sigma$ tension of *Planck* CMB data with weak lensing measurements and redshift surveys [43–45], in the value of S_8 [46]. The tension can be readily visualized as the combination of the amplitude of matter clustering σ_8 in the late universe and the present matter density, Ω_{m_0} , given by $S_8 = \sigma_8 \sqrt{\Omega_{m_0}/0.3}$. Several works [47–62] tried to address these cosmological tensions but could only resolve one tension or the other while maintaining the same number of parameters. The only solutions proposed by [49, 63–72] to resolve all cosmological tensions at present are either highly fine-tuned or involve introducing additional parameters, thereby increasing uncertainties in the parameter space.

Among various proposed solutions, interacting dark sector models [73–84], stand out as potential avenues for addressing tensions related to the H_0 and the S_8 parameter in alternative cosmological frameworks. Motivated by this interesting possibility, we investigate whether interacting dark sector scenarios can mitigate the discrepancies between early- and late-time observational measurements within non-flat cosmology. In this article, while similar aspects have been explored in the past [76], we present two new insights within the dark sector. First, we introduce an additional parameter of spatial curvature within the framework of dark sector interactions that may effectively alleviate or resolve these tensions. Second, we utilize new observational data, including eBOSS DR16 BAO data [85–88] and time-delay strong gravitational lensing measurements from HOLiCOW experiments [89].

The work is organized as follows. The following section explains the model framework, the basic equations and the linear dark matter perturbation evolution equation for the coupled dark sector assuming a non-flat background of the universe. Section 3 describes the observational data and methodology employed in our data analysis pipeline. We present the results obtained in our study in Section 4, and finally, in Section 5, we conclude the findings.

[†]In the appendix, we provide the physical explanation of why and how spatial curvature can help resolve the Hubble tension.

2 INTERACTING DARK ENERGY IN A CURVED UNIVERSE

Assuming the large-scale homogeneous and isotropic space-time, the geometry of the universe is characterized by the Friedmann-Lemaître-Robertson-Walker (FLRW) line element as given by

$$ds^2 = -c^2 dt^2 + a^2(t) \left[\frac{dr^2}{1 - Kr^2} + r^2 d\theta^2 + r^2 \sin^2 \theta d\phi^2 \right]. \quad (1)$$

where ‘ c ’ is the light speed, ‘ $a(t)$ ’ is the scale factor as a function of cosmic time, and ‘ K ’ is the curvature parameter. The values $K = 0, +1, -1$, respectively, denote the universe’s spatially flat, closed, and open geometry. We consider the dark energy as a canonical scalar field ϕ , interacting with cold dark matter element ($\omega_{dm}=0$). Following this assumption, the action for the dark sector interaction can be written as

$$S = \int d^4x \sqrt{-g} \left[\frac{R}{2} - \frac{1}{2} g^{\mu\nu} \partial_\mu \phi \partial_\nu \phi - V(\phi) + \sum_i \mathcal{L}_m^i(\chi_i, \phi) \right]. \quad (2)$$

\mathcal{L}_m is the matter Lagrangian for different matter field elements, which shows ϕ dependency through the coupling. Different matter species (i) may experience different couplings [74, 90]. Our study considers a cosmological scenario where only cold dark matter (CDM) couples to the dark energy (DE) scalar field ϕ by energy or momentum exchange mechanism between them in a non-gravitational way. The other fluids, such as radiation and baryons, are assumed uncoupled to dark energy [91]. The previous study [76] analysed the action integral (Eq. (2)) for $K = 0$ case. Unlike the earlier analysis, here, we perform the analysis for non-zero curvature case.

The variation of Eq. (2) w.r.t. the inverse metric gives Einstein’s gravitational field equation as

$$G_{\mu\nu} = T_{\mu\nu} \equiv T_{\mu\nu}^{(\phi)} + T_{\mu\nu}^{(m)}. \quad (3)$$

where $T_{\mu\nu}$ is the sum of $T_{\mu\nu}^{(\phi)}$ and $T_{\mu\nu}^{(m)}$ which are energy-momentum tensor of DE component and matter component, respectively. By permitting interaction between the dark species, the local conservation equation (Eq. (4)) for CDM and the DE scalar field at the background level become intertwined through a coupling or interaction function Q :

$$-\nabla^\mu T_{\mu\nu}^{(\phi)} = Q_\nu = \nabla^\mu T_{\mu\nu}^{(dm)}, \quad (4)$$

where Q_ν expresses the interaction between dark matter and dark energy

$$Q_\nu = F_{,\phi} \rho_{dm} \nabla_\nu \phi, \quad (5)$$

with $F_{,\phi} \equiv \partial F / \partial \phi$. $F(\phi) = F_0 e^{\beta\phi}$ is the coupling strength and β is a constant. As the radiation component does not interact with dark species, it conserves independently and follows $\nabla^\mu T_{\mu\nu}^{(r)} = 0$. Utilizing the above equations, we obtain the two Friedmann equations for the background evolution as

$$\begin{aligned} \frac{\dot{\phi}^2}{2} + V(\phi) + F(\phi) \rho_{dm} + \rho_r - \frac{3K}{a^2} &= 3H^2, \\ - \left[\frac{\dot{\phi}^2}{2} - V(\phi) + F(\phi) P_{dm} + P_r \right] - \frac{K}{a^2} &= 2\dot{H} + 3H^2. \end{aligned} \quad (6)$$

and the continuity equation for each component as

$$\begin{aligned} \dot{\rho}_\phi + 3H\rho_\phi(1 + \omega_\phi) &= Q, \\ \dot{\rho}_c + 3H\rho_c &= -Q, \\ \dot{\rho}_r + 3H\rho_r(1 + \omega_r) &= 0. \end{aligned} \quad (7)$$

where $H \equiv \frac{\dot{a}}{a}$, represents the time evolution of the universe. The dot indicates derivative w.r.t. time t , and we re-scale the term “ $F(\phi)\rho_{dm}$ ” as ρ_c , denoting the energy density for dark matter coupled to dark energy. Corresponding time part of interaction term in Eq. (5) corresponds to $Q = F_{,\phi}\rho_{dm}\dot{\phi}$. Here, the interaction function Q_v is derived systematically from the action integral and conservation equations, ensuring a robust correlation between dark matter and dark energy. This contrasts with phenomenological fluid models, where the interaction term is introduced ad hoc, without a formal derivation.

The coupling also modifies the matter perturbation evolution equation. In the linearized approximation, assuming the Newtonian gauge, the equation describing the growth of DM density perturbation in the sub-Hubble limit can be expressed as

$$\delta_c'' + \delta_c' \left[2 + \frac{H'}{H} - \frac{F_{,\phi}}{F(\phi)} \phi' \right] - \frac{3}{2} \delta_c \left[\frac{\rho_c}{3H^2} - \frac{1}{3} \phi'^2 \right] \left[1 + \frac{2F_{,\phi}^2}{F(\phi)^2} \right] = 0. \quad (8)$$

where, $\delta_c \equiv \frac{\delta\rho_c}{\rho_c}$ represents the evolution of matter density contrast and the subscript c stands for the CDM component. $\delta\rho_c$ is the perturbed dark matter density. ‘ \prime ’ expresses the derivatives w.r.t. the e-fold, $N = \ln(a)$. The governing equations, both at the background and perturbation levels, determine the dynamics of the interacting scalar field.

Finally, to study the dynamics of the system, we simplify the analysis by formulating autonomous equations through the definition of dimensionless variables as follows:

$$x = \frac{\dot{\phi}}{\sqrt{6}H}, \quad y = \frac{\sqrt{V(\phi)}/3}{H}, \quad \Omega_{dm} = \frac{F(\phi)\rho_{dm}}{3H^2}, \quad \Omega_r = \frac{\rho_r}{3H^2}, \quad \Omega_K = \frac{-K}{a^2H^2}, \quad (9)$$

satisfying the constraint equation:

$$\Omega_\phi + \Omega_{dm} + \Omega_r + \Omega_K = 1. \quad (10)$$

Here, $\Omega_\phi = x^2 + y^2$ represents the density parameter of dark energy. Ω_{dm} and Ω_r represent the density parameters of dark matter and radiation, respectively. Additionally, we define:

$$\lambda = -\frac{V_{,\phi}}{V(\phi)}, \quad m = \frac{F_{,\phi}}{F(\phi)}. \quad (11)$$

These definitions contribute to forming a complete autonomous system. We introduce an additional dimensionless variable ‘ γ ’ to characterize the dark energy equation of state ‘ ω_ϕ ’ as

$$1 + \omega_\phi = \frac{2x^2}{x^2 + y^2} = \gamma. \quad (12)$$

Operating derivative with respect to number of e-folding $N = \ln(a)$ on above variables, Eqs. (9), (11), and (12), we can obtain the coupled dynamical set of equations within curved cosmology. During the dynamical analysis, we assumed an exponential potential, $V(\phi) \propto e^{-\lambda\phi}$ (where λ is a constant), which results in the equation corresponding to λ simplifying to $\lambda' = 0$. Similarly, for the coupling term $F(\phi) \propto e^{\beta\phi}$, $m' = 0$. These simplifications lead to the 4D system describing background dynamics, which can be expressed as

$$\begin{aligned} \Omega_\phi' &= 3(1 - \gamma)\Omega_\phi(1 - \Omega_\phi) + \Omega_\phi\Omega_r + m\Omega_{dm}\sqrt{3\gamma\Omega_\phi} - \Omega_\phi\Omega_K, \\ \Omega_r' &= \Omega_r(\Omega_r - 1) + 3\Omega_r\Omega_\phi(\gamma - 1) - \Omega_r\Omega_K, \\ \Omega_K' &= -\Omega_K(\Omega_K - 1) + 3\Omega_K\Omega_\phi(\gamma - 1) + \Omega_r\Omega_K, \\ \gamma' &= (2 - \gamma)\sqrt{3\gamma\Omega_\phi} \left(-\sqrt{3\gamma\Omega_\phi} + \lambda\Omega_\phi + m\Omega_{dm} \right). \end{aligned} \quad (13)$$

The initial condition on ω_ϕ is $\omega_\phi \approx -1$, i.e., $\gamma \simeq 0.0001$ [92]. Other parameters, namely Ω_ϕ , Ω_r , Ω_K , λ , and m , are kept as free parameters.

DM density perturbation equation Eq. (8) describing the perturbed dynamics can now be written as

$$\delta_c'' = -\left(\frac{1}{2} - \frac{3}{2}\Omega_\phi(\gamma-1) - \frac{1}{2}\Omega_r + \frac{1}{2}\Omega_K - m\sqrt{3\gamma\Omega_\phi}\right)\delta_c' + \frac{3}{2}\left(1 - \Omega_\phi(1+\gamma) - \Omega_r - \Omega_K\right)(1+2m^2)\delta_c. \quad (14)$$

To ensure the universe's evolution around the matter-dominated epoch, we assume the time evolution at $N_i = -7$. Hence, we put the initial conditions as $\phi(N_i) = \phi'(N_i) = 0$ and $\delta_c(N_i) = \delta_c'(N_i) = 10^{-3}$. Combining Eq. (13) and Eq. (14), background and perturbed set of equations, we constrain the model and its parameters using the cosmological observations as described in the next section.

3 OBSERVATIONAL DATA AND METHODOLOGY

In this section, we present the latest observational data from diverse sources used to investigate and constrain model parameters in the case of interactions with curvature.

- **CMB:** In the present analysis, we consider the CMB distance priors from the final *Planck* CMB data obtained by Chen et al [93]. In particular, we have used *Planck* 2018 compressed CMB likelihood TT, TE, EE + lowE [94].

Note that we employ CMB distance priors for the efficient and self-consistent approach they offer in exploring the parameter space of our model. The distance priors have been effectively used to study the late-time universe and implemented to replace global fitting of the full *Planck* 2018 data for dark energy models beyond standard Λ CDM [93, 95–100]. However, it is important to note that these priors may not fully capture the complexities of the full CMB power spectrum due to hidden assumptions, particularly in cases of significant deviations from the Λ CDM model, which may lead to systematic offsets in cosmological parameters [100, 101]. This assumption underlies our analysis. Thus, we clarify that the constraints derived from our work are based on the premise that the distance priors adequately represent the relevant features of the full CMB data in this case.

- **BAO:** For BAO distance measurements, we use data points from different experiments that include isotropic BAO measurements at small redshifts from 6dF [102] and SDSS DR7-MGS surveys [103], as well as at high redshifts from SDSS DR14-eBOSS quasar clustering [104] and cross-correlation of $\text{Ly}\alpha$ with quasars from SDSS DR12 [105]. Additionally, we consider anisotropic BAO measurements by BOSS DR12 galaxy sample [106]. We also added eBOSS DR16 data on emission line galaxies (ELG), luminous red galaxies (LRGs), and Quasar samples [85–88]
- **Cosmic Chronometers (CC):** We also include the measures of $H(z)$ using the CC covariance matrix [107–109] which measures the Hubble evolution in an independent way.
- **PantheonPlus (PP) & SH0ES:** We include SNe-Ia measurements from the Pantheon+ compilation which contains 1701 light curves of 1550 distinct SNe-Ia in the redshift range $z \in [0.001, 2.26]$ [110, 111], referred to as PantheonPlus (PP). This sample also includes SH0ES Cepheid-calibrated host galaxy distance [42], denoted as R21. Thus, for the measurement of H_0 , the SH0ES Cepheid host distance covariance matrix along with PP, we use the modified likelihood (refer Eq. 15 of [111]), enabling us to place constraints on H_0 .
- **MASERS:** We add the measurement of H_0 from Masers galaxy samples, UGC 3789, NGC 5765b, and NGC 4258 in the Hubble flow redshifts $z = 0.0116, 0.0340, \text{ and } 0.0277$ respectively [112–116].
- **Growth rate data ($f\sigma_8$):** In addition to geometric probes, to investigate the matter density perturbations, we use growth rate data ($f\sigma_8$) measured from Redshift-space distortions (RSDs), as collected in [117].

- **Strong Gravitational Lensing Time Delay (SLTD)** We also add observations of the Hubble constant H_0 from time-delay gravitational lensing as measured by HOLiCOW experiments [89].

To constrain the parameter space of the interaction with curvature (Coupled+ Ω_K) cosmological scenario, we implement a modified version of the Markov Chain Monte Carlo (MCMC) code, emcee: the MCMC Hammer [118] package. Table 1 lists the priors imposed on the cosmological parameters. During the analysis, the Hubble constant is assumed to be $H_0 = 100h \text{ km s}^{-1} \text{ Mpc}^{-1}$, where h is a dimensionless parameter. The baryon density parameter, Ω_{b_0} , and the spectral index, n_s are fixed at 0.045 and 0.96, respectively, according to *Planck* (2018) [26]. It should be noted that we have employed positive priors on the interaction parameter. However, the results remain unchanged even if we opt for negative or larger priors instead.

<i>Parameters</i>	<i>Priors</i>
$\Omega_{\phi_i} * 10^{-9}$	[0.05, 4.0]
Ω_{r_i}	[0.09, 0.19]
λ_i	[10^{-4} , 3.0]
m_i	[10^{-6} , 0.08]
h	[0.4, 1.0]
r_{drag}	[120, 180] Mpc
σ_8	[0.5, 1.0]
Ω_K	[-1.0, 1.0]
M	[-21.0, -18.0]

Table 1: Flat priors on the cosmological parameters used in this analysis.

4 RESULTS AND DISCUSSION

We present in Table 2 the results obtained within the coupled and curved cosmology (Coupled+ Ω_k) for four observational data combinations. We present the mean and 1σ bounds (68% confidence levels (CL)) on the different cosmological parameters for the ***BASE*** combination, representing ‘*BAO+CMB+CC+f σ_8* ’. ***BASE*** combination represent our baseline data. We subsequently add ‘*Masers and PantheonPlus (PP)*’, ‘*SLTD*’, and ‘*H₀*’ data to the ***BASE*** combination to study their effects on parameter constraints. The corresponding contour plots and 1D marginalized posterior distribution for different cosmological parameters are shown in Fig. 1.

4.1 Model Parameters in Coupled+ Ω_k

The parameter λ_i indicate how steeply the potential associated with the dark energy field, ϕ changes. The effect of variations in λ_i can be seen on dark energy equation of state (DE EoS) parameter ω_ϕ , representing dark energy evolution, and cosmic structure formation and growth parameter, S_8 , as shown in Table 2. Higher λ_i value ($0.90^{+0.35}_{-0.82}$) for ***BASE*** data combination indicates corresponding higher ω_ϕ value. Whereas lower λ_i ($0.55^{+0.22}_{-0.50}$), for ‘***BASE+Masers+PP+SLTD***’ combination indicates lower ω_ϕ value (more negative) for the same data combination. Similar effects are observed on structure growth parameter S_8 , indicating higher S_8 for higher λ_i and lower S_8 for low λ_i values for the same data combination. We also found that the coupling parameter m_i , peaks at the low value, for all the four data combinations, as shown in Table 2. This small coupling magnitude indicates preference for a significantly weak interaction between dark energy and dark matter by the cosmological datasets in the Coupled+ Ω_K case. However, these findings are model-dependent and may vary for other coupling models.

<i>Parameters</i>	<i>BASE</i>	<i>+Masers +PantheonPlus (PP)</i>	<i>+Masers+PP +SLTD</i>	<i>+Masers+PP +SLTD+H₀</i>
$\Omega_{\phi_i} * 10^{-9}$	0.89±0.25	0.92 ^{+0.29} _{-0.23}	0.92 ^{+0.30} _{-0.24}	0.90 ^{+0.29} _{-0.24}
Ω_{r_i}	0.157±0.014	0.153 ^{+0.011} _{-0.010}	0.150 ^{+0.012} _{-0.010}	0.134±0.006
λ_i	0.90 ^{+0.35} _{-0.82}	0.55 ^{+0.21} _{-0.51}	0.55 ^{+0.22} _{-0.50}	0.58 ^{+0.22} _{-0.54}
m_i	0.0011 ^{+0.00039} _{-0.00110}	0.0012 ^{+0.00047} _{-0.00110}	0.0012 ^{+0.00049} _{-0.00110}	0.0013 ^{+0.00050} _{-0.00110}
S_8	0.779 ^{+0.027} _{-0.026}	0.766 ^{+0.023} _{-0.024}	0.764±0.023	0.768±0.024
Ω_{dm}	0.341 ^{+0.0141} _{-0.0143}	0.328 ^{+0.0086} _{-0.0085}	0.327 ^{+0.0087} _{-0.0088}	0.330 ^{+0.0104} _{-0.0105}
ω_ϕ	-0.931 ^{+0.065} _{-0.066}	-0.971 ^{+0.027} _{-0.030}	-0.971 ^{+0.026} _{-0.029}	-0.969 ^{+0.029} _{-0.032}
h	0.655 ^{+0.038} _{-0.042}	0.665 ^{+0.026} _{-0.030}	0.674 ^{+0.028} _{-0.032}	0.717±0.015
r_{drag} (Mpc)	142.3 ^{+7.5} _{-8.8}	141.9±6.0	140.0±6.2	131.0±2.9
Ω_k	0.0062±0.0046	0.0040 ^{+0.0035} _{-0.0031}	0.0037±0.0033	0.0050±0.0038
$\Delta\chi^2_{min}$	15.091	6.690	-1.269	0.321
ΔAIC	19.091	10.690	2.730	4.321

Table 2: Mean values with 1σ bound (68% CL) on the parameters within the **Coupled+ Ω_K** scenario from various datasets. The $\Delta\chi^2_{min}$ and ΔAIC are calculated with respect to the Λ CDM+ Ω_K model for the very same dataset. The negative values indicate the preference for the Coupled+ Ω_K case, while the positive values for the Λ CDM+ Ω_K case. Here, ‘**BASE**’ represents ‘*BAO+CMB+CC+f σ_8* ’ dataset.

4.2 The H_0 Tension

In the curved cosmology analysis presented in Table 2, we have found, that ‘*BAO+CMB+CC+f σ_8* ’ (*BASE*) constrains H_0 to $65.5^{+3.8}_{-4.2}$ km/s/Mpc at 68% CL, which is 0.4σ away from *Planck* 2018 + Λ CDM results ($H_0 = 67.37 \pm 0.54$ km/s/Mpc) [26] (hereafter ‘*Planck* 2018 + Λ CDM results’ will be referred to as ‘P18+ Λ CDM’ collectively). However, the same H_0 constraints indicate a 1.5σ difference with the SH0ES determination of H_0 ($H_0 = 73.04 \pm 1.01$ km/s/Mpc) [42] (hereafter ‘SH0ES determination of H_0 ’ will be referred to as ‘R21’). This improvement in the Hubble constant, H_0 value, which shifts H_0 towards the R21 value within 1.5σ , is primarily due to an increased volume in the parameter space rather than an actual rise in the mean value of H_0 . With each addition to the *BASE* dataset, the constraints strengthen and the mean value shifts towards the R21 value, maintaining the tension with R21 at the level of $\sim 1.7\sigma$. When the SH0ES constraint is included (last column of Table 2), the fit is increased to $H_0 = 71.7 \pm 1.5$ km/s/Mpc, indicating a less than 2.2σ deviation from P18+ Λ CDM and a 0.6σ shift towards R21. These findings are also evident in Fig. 1. We noticed that the H_0 results obtained from fitting the ‘Coupled+ Ω_k ’ model using the dataset ‘*BASE+Masers+PP+SLTD+H₀*’ demonstrate slight reductions in difference with both P18+ Λ CDM [26] and R21 [42] analyses compared to the results found in the flat case interacting model discussed in [76].

4.3 The S_8 Tension

In the S_8 analysis, the *BASE* estimates S_8 to $0.779^{+0.027}_{-0.026}$, with 1.4σ away from P18+ Λ CDM ($S_8 = 0.830 \pm 0.013$) [26]. However, this shift in S_8 measurement is less than 0.5σ towards lensing observation estimates [43, 119]. The Masers and PantheonPlus addition to *BASE* further provides unprecedented precision on S_8 , preferring lower S_8 ($S_8 = 0.766^{+0.023}_{-0.024}$), with a shift towards DES-Y3 estimates [119] ($S_8 = 0.776 \pm 0.017$) by less than 0.3σ and deviation from P18+ Λ CDM by 1.8σ .

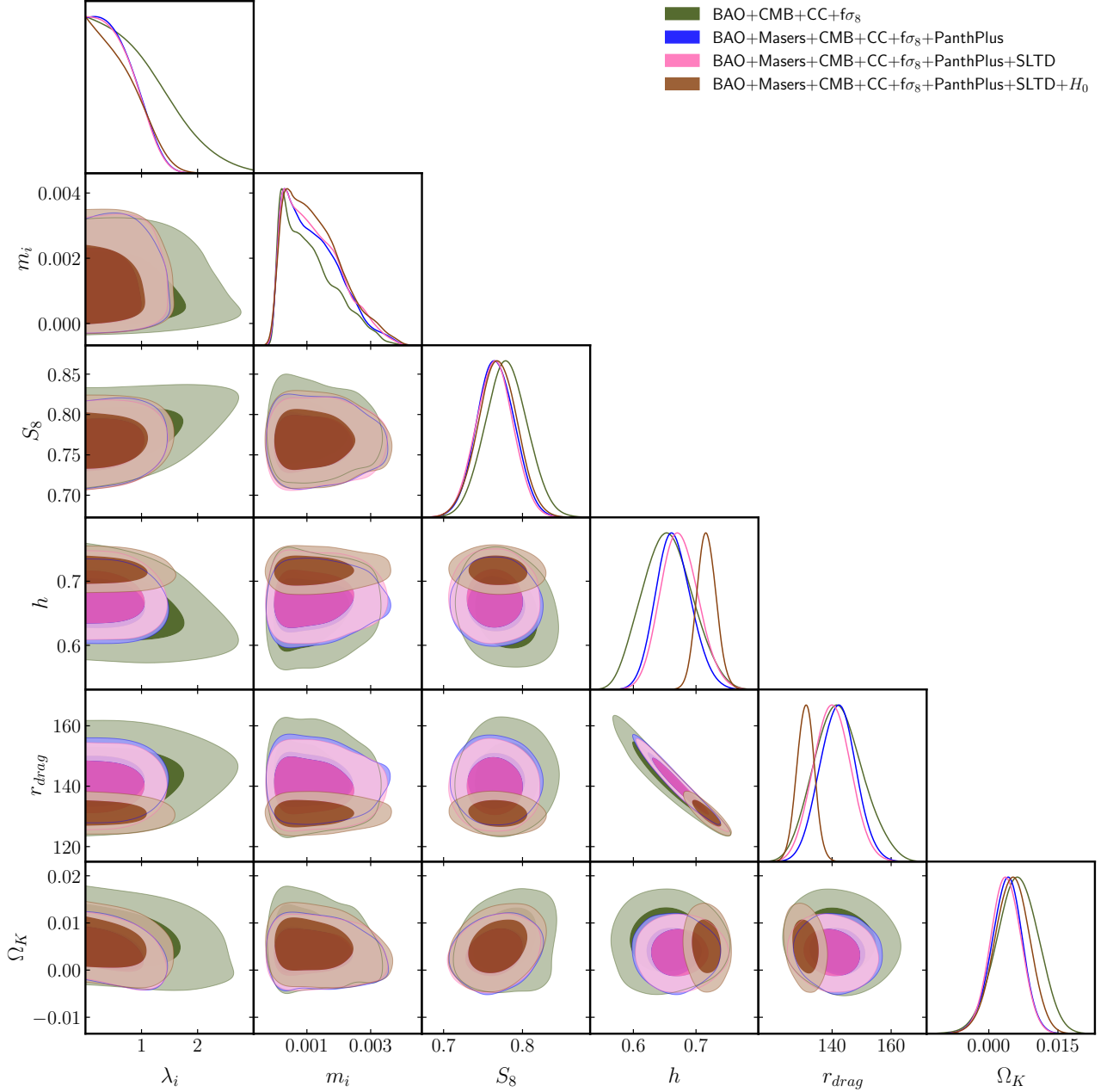


Figure 1: Contour plots at 68% and 95% CL and corresponding 1D marginalized posterior distributions for the most important parameters obtained from the MCMC analysis within the present **Coupled+ Ω_K** cosmological scenario across various data combinations.

We noticed that for this combination, the S_8 estimates closely aligns with the value from KiDS-1000-BOSS ($S_8 = 0.766^{+0.020}_{-0.014}$) [43]. The inclusion of SLTD (third column of Table 2) predicts lower S_8 value than any other dataset shown in Table 2. By considering the combined analysis ‘*BASE+Masers+PP+SLTD+ H_0* ’ (all data), we find $S_8 = 0.768 \pm 0.024$. This value indicates a reduced difference within 2σ range from P18+ Λ CDM [26], compared to the 2.5σ discussed in the flat case interacting model [76]. Notably, this S_8 value is very close to those from DES-Y3 [119] (within 0.2σ) and KiDS-1000-BOSS [43] (within 0.1σ), improving upon the 0.5σ and 0.3σ differences observed in the flat case interacting model [76]. Note that even though we have not used the KiDS-1000-BOSS and DES-Y3 survey results while performing the Coupled+ Ω_K model analysis, the S_8 derived with the Coupled+ Ω_K framework are qualitatively same as the one obtained by using the KiDS-1000-BOSS and DES-Y3 data in their models [43, 119].

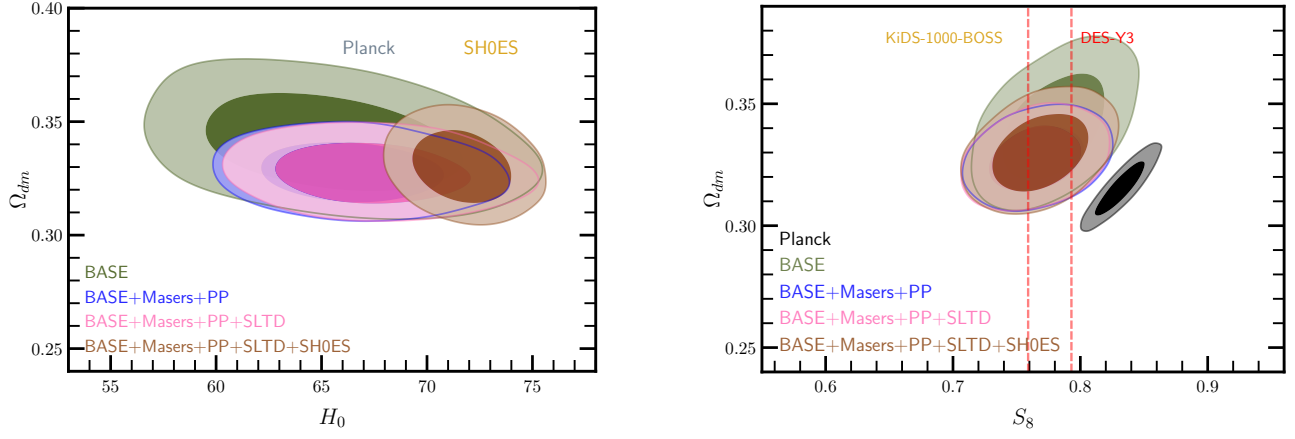


Figure 2: **Left:** 68% and 95% CL constraints on H_0 - Ω_{dm} parameter space from various datasets shown in the figure for Coupled+ Ω_K scenario. The ‘Gray’ and ‘Golden’ bands represent the 68% CL constraints on H_0 from *Planck* and SH0ES analyses, respectively. **Right:** 68% and 95% CL constraints on S_8 - Ω_{dm} parameter space from various datasets shown in the figure for Coupled+ Ω_K scenario. The ‘Golden’ band and ‘Red-dashed’ line represent the 68% CL constraints on S_8 from KiDS-1000-BOSS and DES-Y3 analyses, respectively. The ‘Black’ contours show 68% and 95% CL on S_8 from *Planck* 2018.

4.4 Parameter Correlations in Coupled+ Ω_K

We also observed the change in Ω_K for each dataset. These changes in Ω_K are associated with the relative shifts in S_8 and Ω_{dm} (as shown in Table 2), indicating a slightly higher value of $\Omega_{dm} = 0.341^{+0.0141}_{-0.0143}$ and $S_8 = 0.779^{+0.027}_{-0.026}$ corresponding to higher Ω_K ($\Omega_K = 0.0062 \pm 0.0046$) for the *BASE* data combination and a shift towards lower value of $\Omega_{dm} = 0.327^{+0.0087}_{-0.0088}$ and $S_8 = 0.764 \pm 0.023$ corresponding to lower Ω_K ($\Omega_K = 0.0037 \pm 0.0033$) for ‘*BASE+Masers+PP+SLTD*’ combination, with more precise constraints. The S_8 and Ω_{dm} correlation results are presented in the right panel of Fig. 2. It is to be noted that the S_8 results presented in subsection 4.3 show a difference of $\sim 1.4\sigma$ for the *BASE* dataset and $\sim 2\sigma$ for the ‘*BASE+Masers+PP+SLTD+H_0*’ dataset from the P18+ Λ CDM. However, when examining the S_8 - Ω_{dm} contour plots (Fig. 2, right panel), the difference in those contours exceeds 2σ from the *Planck* CMB contour. This increase in the difference appeared from the correlation between S_8 - Ω_{dm} . Furthermore, due to the anti-correlation between H_0 and the dark matter density parameter Ω_{dm} , we noticed the Ω_{dm} transition from higher to lower values correspond to lower to higher values of H_0 , excepts for the combined analysis ‘*BASE+Masers+PP+SLTD+H_0*’, as shown in Table 2. In this case, the lack of correlation between H_0 and Ω_{dm} indicates their independent evolution, effectively breaking the degeneracy for the combined analysis (the last column of Table 2). These results are presented in the left panel of Fig. 2.

Similarly, the lack of correlation is also observed in H_0 and Ω_K parameter space for the ‘*BASE+Masers+PP+SLTD+H_0*’ dataset. Additionally, we noticed the high H_0 value correspond to positive Ω_K for the combined analysis ‘*BASE+Masers+PP+SLTD+H_0*’, similar to the trend observed in the Λ CDM+ Ω_K model (refer Table 3). This indicates that, despite the added complexity introduced by the coupling and curvature parameter, the relationship between H_0 and Ω_K remains consistent, favoring a slightly positive curvature parameter for higher H_0 , as shown in the last column of Table 2.

4.5 The Ω_K and the Impact on ω_ϕ

Now, we investigate the curvature parameter, Ω_K and how it affects the dark energy equation of state parameter, ω_ϕ constraints. In the ‘Coupled+ Ω_K ’ model, for ‘*BASE*’ dataset we get an evidence of an open Universe with the constraint on the curvature parameter reading $\Omega_k = 0.0062 \pm 0.0046$ and a non-zero coupling strength at 68 % CL. In this case, the corresponding ω_ϕ is found to be $\omega_\phi = -0.931^{+0.065}_{-0.066}$, which is moderately higher than the ω_ϕ obtained in other datasets presented in Table 2.

The preference for the curved spacetime is found to be consistent at 68% CL for ‘*BASE+Masers+PP*’, ‘*BASE+Masers+PP+SLTD*’, and ‘*BASE+Masers+PP+SLTD+H₀*’ combinations, with only a mild indication for the presence of coupling in the dark sector. As Ω_k prefers lower values, we noticed more negative values of ω_ϕ for all these data combinations compared to the *BASE* combination. Also, the constraint on Ω_k from the ‘*BASE+Masers+PP+SLTD*’ ($\Omega_k = 0.0037 \pm 0.0033$) is more precise than those obtained using other datasets. This improved precision is reflected in the tighter constraints on ω_ϕ ($\omega_\phi = -0.971^{+0.026}_{-0.029}$), shown in the fourth column of Table 2, which is in perfect agreement with the cosmological constant case ($\omega_\phi = -1$) at 68% CL.

When analyzed, we found that the ω_ϕ values, in the ‘Coupled + Ω_K ’ scenario, are lower, compared to those obtained in the flat interacting scenario in [76]. However, the estimates of ω_ϕ derived from both the ‘Coupled + Ω_K ’ scenario and the flat interacting scenario are within $\sim 1\sigma$ bounds of each other. We have also shown the comparison of our result with the previous works on the constraints of ω_ϕ in Fig. 3 for ‘*BAO+Masers+CMB+CC+f σ_8 +PP*’ dataset, where ω_ϕ is found to be ($\omega_\phi = -0.9422^{+0.0485}_{-0.0475}$) in flat interacting model.

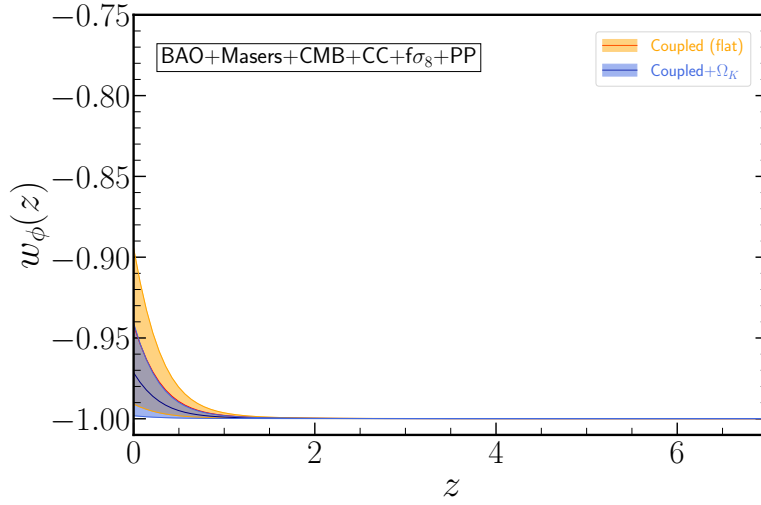


Figure 3: Evolution of the dark energy equation of state parameter $\omega_\phi(z)$ with respect to redshift for (flat) coupled and Coupled+ Ω_K scenarios. The orange and blue regions represent the 68% CL on $\omega_\phi(z)$ for the flat coupled and Coupled+ Ω_K cases, respectively, using the ‘*BAO+Masers+CMB+CC+f σ_8 +PP*’ combination.

4.6 Model Probability Assessment

Finally, we discuss the comparison between the Coupled+ Ω_K model and the Λ CDM+ Ω_K model in Table 2. We compare the minimum χ^2 and Akaike information criterion (AIC) values obtained for each model across the respective datasets, where $AIC = \chi^2_{\min} + 2 \times d$, and d is the number of parameters in the model. The lowest chi-squared and AIC values indicate the best-fitting model, closely matching the measured data. In Table 2, negative values of $\Delta\chi^2_{\min}$ and ΔAIC indicate a preference for the Coupled+ Ω_K model, while positive values indicate a preference for the Λ CDM+ Ω_K model. With a positive ΔAIC , we observed higher values of AIC for the Coupled+ Ω_K model compared to the Λ CDM+ Ω_K framework. This suggests that the Coupled+ Ω_K model provides a weaker fit to the observational data across all dataset combinations, and is therefore disfavored by the AIC approach. Furthermore, in the ‘*BASE+Masers+PP+SLTD*’ case, $\Delta\chi^2_{\min} = -1.269$ indicates preference for Coupled+ Ω_K model over Λ CDM+ Ω_K . However, based on the value of $\Delta AIC = 2.730$ for this dataset, the Λ CDM+ Ω_K model exhibits better concordance with the data, indicating no preference for Coupled+ Ω_K one. These inconclusive results are insufficient to definitively favor one model over the other, particularly for the ‘*BASE+Masers+PP+SLTD*’ dataset.

4.7 Cosmological Constraints from Different Models

We now compare the constraints on the cosmological parameters obtained from five different models: flat Λ CDM (denoted by Λ CDM (Flat)), Λ CDM+ Ω_k , Un-coupled+ Ω_k , Coupled+ Ω_k , and flat coupled (denoted by Coupled (Flat)) for the ‘*BASE+Masers+PP+SLTD+H₀*’ combination, as shown in Table 3. Here, Λ CDM+ Ω_k represents the Λ CDM framework in a curved universe, and Un-coupled+ Ω_k represents a scenario without coupling (interaction), where the coupling parameter m_i in the Coupled+ Ω_k model is set to zero.

<i>Parameters</i>	Λ CDM (Flat)	Λ CDM+ Ω_k	Un-coupled+ Ω_k	Coupled+ Ω_k	Coupled (Flat)
S_8	0.754 ± 0.022	0.774 ± 0.024	0.758 ± 0.024	0.768 ± 0.024	0.761 ± 0.023
Ω_{dm}	0.318 ± 0.0073	0.335 ± 0.0110	$0.331^{+0.0104}_{-0.0103}$	$0.330^{+0.0104}_{-0.0105}$	$0.322^{+0.0081}_{-0.0082}$
h	0.722 ± 0.013	0.717 ± 0.013	0.718 ± 0.015	0.717 ± 0.015	0.718 ± 0.016
r_{drag} (Mpc)	132.1 ± 2.5	131.6 ± 2.6	130.7 ± 3.0	131.0 ± 2.9	132.0 ± 3.0
Ω_k	-	0.0510 ± 0.0180	0.0056 ± 0.0037	0.0050 ± 0.0038	-
m_i	-	-	-	$0.0013^{+0.00050}_{-0.00110}$	$0.0014^{+0.00060}_{-0.00120}$
$\Delta\chi^2_{min}$	0	-4.869	28.351	-4.548	25.099
ΔAIC	0	-2.869	32.351	1.451	29.099

Table 3: Mean values with 1σ bound obtained on the most relevant parameters within the Λ CDM (Flat), Λ CDM+ Ω_k , Un-coupled+ Ω_k , Coupled+ Ω_k , and Coupled (Flat) scenarios for ‘*BASE+Masers+PP+SLTD+H₀*’ dataset. The $\Delta\chi^2_{min}$ and ΔAIC are calculated with respect to the Λ CDM model. The sign convention is same as in Table 2.

In our analysis, we observed that the H_0 estimates in the flat Λ CDM and Λ CDM+ Ω_K models are approximately 1.2 times more precise than those in the other three modeling scenarios, as shown in Table 3. However, these estimates exhibit a $\sim 2.7\sigma$ difference from the P18+ Λ CDM result [26]. In contrast, the Un-coupled+ Ω_K , Coupled+ Ω_K , and Coupled (Flat) models show a $\sim 2.2\sigma$ difference with P18+ Λ CDM. The constraints obtained on H_0 align more closely with the R21 result [42] and remain consistent across all models within 0.6σ , except for the Λ CDM+ Ω_k model, where $H_0 = 71.7 \pm 1.3$ km/s/Mpc indicates a 1σ deviation from the R21 value. Please note that the derived H_0 is higher for all models in Table 3, so the Coupled+ Ω_k model is not an exception. Similarly, the constraints on S_8 in the flat Λ CDM model exhibit better precision (a lower and a well-constrained S_8 estimation) than those in the other four models, as shown in Table 3. In this case, S_8 has a lower value (0.754 ± 0.022 at 68% CL), shifting it 2.2σ away from P18+ Λ CDM [26], $\sim 0.7\sigma$ closer to DES-Y3 [119], and $\sim 0.3\sigma$ closer to KiDS-1000-BOSS [43]. Consequently, the Λ CDM+ Ω_k bounds on S_8 are 0.774 ± 0.024 at 68% CL, showing a slight decrease in the difference (1.6σ) with P18+ Λ CDM compared to the flat Λ CDM case (as discussed previously). Additionally, this analysis shows close alignment with DES-Y3 (0.1σ) while S_8 retaining its consistency of $\sim 0.3\sigma$ with KiDS-1000-BOSS survey as in the flat Λ CDM model[‡].

We also observed that the curvature density parameter, Ω_K , indicates a preference for an open universe in the Λ CDM+ Ω_K case which is found to be $\Omega_K = 0.0510 \pm 0.0180$ at 68% CL (third column of Table 3). This preference for a curved spacetime persists in Un-coupled+ Ω_K and Coupled+ Ω_K scenarios, with significant reduction in Ω_K values (both mean and error bars) compared to Λ CDM+ Ω_K . These precise constraints narrow down the Ω_K parameter space. The effects of curvature are also

[‡]Note that the slight difference in parameter constraints in Coupled (Flat) model, in Table 3 are due to the addition of new datasets, SLTD and BAO SDSS DR16, which were not considered in our previous study [76] for the flat case interacting model.

witnessed on the parameters S_8 and Ω_{dm} in Table 3. In the flat Λ CDM model, the absence of Ω_K indicates tightened constraints on S_8 and Ω_{dm} , while the introduction of curvature broadens the parameter space for these parameters in Λ CDM+ Ω_K , Un-coupled+ Ω_K , and Coupled+ Ω_K models. The DM density parameter reading $\Omega_{dm} = 0.322^{+0.0081}_{-0.0082}$ at 68% CL in the flat coupled case, we observed moderate broadening in the parameter space compared to the flat Λ CDM model due to the effect of coupling complexities. However, this constraint is still better than that obtained in the other three scenarios where the curvature component is included.

In this analysis, the model comparison statistics are computed relative to the flat Λ CDM using the ‘*BASE+Masers+PP+SLTD+H₀*’ dataset. We noticed that with $\Delta AIC = -2.869$, the Λ CDM+ Ω_K model fits the observations better than other models presented in Table 3 and the same is also preferred over the flat Λ CDM. In addition, positive values of both, $\Delta\chi_{min}^2$ and ΔAIC in Un-coupled+ Ω_K and Coupled (Flat) cases show that the data significantly prefer the flat Λ CDM picture over these models. We also noted that the $\Delta\chi_{min}^2$ in the Coupled+ Ω_K model is negative. However, this does not indicate a preference for this model over the flat Λ CDM one, as can be inferred from the value of ΔAIC ($\Delta AIC > 0$) shown in the fifth column of Table 3.

5 CONCLUSIONS

In this paper, we study an extension of the coupled dark energy-dark matter model having dynamic interaction $Q = F_{,\phi} \rho_{dm} \dot{\phi}$ by introducing curvature component in the universe. We aim to investigate the effects of curvature on the coupled quintessence model and its associated (free and derived) parameters, in particular H_0 and S_8 .

We tested our model with several combinations of data and analyzed the influence of each dataset on the cosmological parameters. Though weak, we observed a coupling which is different from zero today. We noticed large error bars in computing the H_0 value from *BASE* combination. These error bars are reduced with the addition of ‘*Masers+PP*’ data to the previous dataset. With further addition of ‘*SLTD*’ and SH0ES’ ‘ H_0 ’ data, the mean value is increased, shifting the consistency more towards the R21 analysis. The S_8 is well constrained for all the datasets considered in this analysis in Table 2. The addition of subsequent data shows S_8 consistency more toward the large-scale structure observations. We also mentioned the dark matter energy density Ω_{dm} parameter and presented its respective correlation with H_0 and S_8 , in terms of H_0 - Ω_{dm} and S_8 - Ω_{dm} planes in Fig. 2. Furthermore, the bounds on Ω_K preferred an open Universe at 68% CL under the *BASE* dataset in Table 2, and this preference for the curved Universe remains the same for all other data considerations. Later, we presented the impact of the curvature component on the time evolution of the DE EoS parameter, ω_ϕ in Sec. 4.5 and shown the comparison between flat coupled and Coupled+ Ω_K models in Fig. 3. While measuring the goodness of fit of the Coupled+ Ω_K model to the data with respect to the Λ CDM+ Ω_K in Table 2, we have found no evidence in favor of Coupled+ Ω_K by any of the data combinations. Here, the fit determined by AIC indicates a preference for the Λ CDM+ Ω_K framework because $\Delta AIC > 0$ in all cases.

In the end, we presented and compared the cosmological constraints obtained from different model analyses in Table 3. In all models that we considered, we found that the Hubble tension parameter, H_0 indicates close alignments with R21 analysis, except 1σ deviation in the Λ CDM+ Ω_K model due to its ability of finding a lower and precise constraint on H_0 than any other models, as shown in Table 3. Also, we found that the matter structure growth parameter, S_8 , in the Λ CDM+ Ω_K model shows quite a negligible difference with DES-Y3 results, and in this case, the model is favored over Λ CDM ($\Delta\chi_{min}^2 = -4.869$ and $\Delta AIC = -2.869$). We found the similar constraints on S_8 (within 0.2σ bounds with DES-Y3 and KiDS-1000-BOSS survey results) when analysing Coupled+ Ω_K case, using the combined analysis ‘*BASE+Masers+PP+SLTD+H₀*’. However, in this case, the model is not favored by the data because $\Delta AIC = 1.451$, even though we obtained $\Delta\chi_{min}^2 = -4.548$.

Following the above analyses, we noticed that the coupled case, with the presence of non-zero curvature (Coupled+ Ω_K model), can provide a compelling solution to the H_0 and S_8 tensions. Even from the model comparison perspective, we found that the coupled+ Ω_K model, using all the dataset

has a chance to better fit the observations ($\Delta\chi_{min}^2 = -4.548$) and can be a preferred model relative to the flat Λ CDM framework (Table 3). Besides this, considering the data analyses of model under assumption, our study demonstrates how the interaction between dark energy and dark matter within non-zero spatial curvature framework modifies the universe's dynamics. This includes the timing of dark energy dominance, its substantial effects on late-time accelerated expansion, and its role in structure formation and clustering, as reflected in parameters like S_8 . These results reveal that observed cosmological tensions can be attributed to either modifications in the universe's geometry (spatial curvature) or interactions within the dark sector or both. Specifically, while the spatial curvature influences the cosmic energy budget and modifies the Hubble parameter and structure growth rate, interaction strength affects the equation of state for dark energy (ω_{de}) and dark matter clustering. These effects, together, suggest that it may be better to relax the flatness assumption and the cosmological constant nature of dark energy when analyzing cosmological models, as they could provide solutions to a number of cosmological tensions. In this context, further in-depth research is needed at both theoretical and observational levels to establish the interaction model as a promising cosmological model, since such an interaction may lead to modifications in the clustering patterns of large-scale structures, potentially affecting clustering strength at various scales. To draw more robust conclusions, we need to improve upon the statistical errors, which can be achieved by including data from future high-quality observations such as from Euclid [120] and DESI [39, 121] surveys that promise enhanced precision for cosmological parameter measurements [122–124]. In the future, we also plan to perform further analysis with other forms of interacting dark energy, such as phantom one, and use DESI BAO data which could further help alleviate these discrepancies.

ACKNOWLEDGMENTS

We thank the anonymous referee for his/her thoughtful remarks and suggestions which led to material improvements in the manuscripts. We are grateful to Ruchika for her assistance during the computational part and for further discussion. This work is partially supported by DST (Govt. of India) Grant No. SERB/PHY/2021057.

Data availability: No data is associated with the manuscript.

APPENDIX

The following explains the Hubble evolution dependence on spatial curvature and dark sector coupling.

The measurement of the angular scale of the sound horizon ($\theta_s = r_s(z_{dec})/D_A(z_{obs})$) infers the Hubble expansion parameter, H_0 , under the assumption of a given cosmological model. Here, $r_s(z_{dec})$ is the comoving sound horizon at the redshift z_{dec} at which photons and baryons decouple, and $D_A(z_{obs})$ is the comoving angular diameter distance to the observation. $D_A(z_{obs})$ depends on the redshift-dependent expansion rate $H(z)$, as $D_A(z_{obs}) = \frac{1}{H_0} \int_0^{z_{obs}} \frac{dz}{E(z)}$, where $E(z)$ incorporates contributions from matter, curvature, and dark energy components, i.e. $E(z) = \sqrt{\Omega_m(1+z)^3 + \Omega_K(1+z)^2 + \Omega_{de}(z)}$ $= \frac{H(z)}{H_0}$. To achieve a high H_0 value ($\sim 73 \text{ Km/s/Mpc}$) consistent with local measurements [42], the late-universe solution ($z \leq 2$) requires modification involving new physics. While dynamical dark energy or interaction among dark sector components can alter the Hubble expansion rate, incorporating an ingredient in the form of spatial curvature offers an additional degree of freedom. This allows H_0 to approach a higher value today while preserving the integrated distance D_A . This may help to understand and find solution to the H_0 tension. Additionally, the spatial curvature can also alter the growth of density perturbations by modifying overall expansion rate, leading to reduce the discrepancy in the growth parameter S_8 between high-redshift (CMB) [26] and low-redshift (weak lensing, galaxy clustering) [43–45] observations.

REFERENCES

- [1] G. Hinshaw *et al.*, “Nine-year wilkinson microwave anisotropy probe (wmap) observations: Cosmological parameter results,” *The Astrophys. J. Suppl. Series*, vol. 208, p. 19, sep 2013.
- [2] A. Balbi *et al.*, “Constraints on cosmological parameters from MAXIMA-1,” *Astrophys. J. Lett.*, vol. 545, pp. L1–L4, 2000.
- [3] C. J. MacTavish *et al.*, “Cosmological parameters from the 2003 flight of BOOMERANG,” *Astrophys. J.*, vol. 647, pp. 799–812, 2006.
- [4] A. Melchiorri *et al.*, “A measurement of omega from the north american test flight of boomerang,” *The Astrophysical Journal*, vol. 536, p. L63, jun 2000.
- [5] P. A. R. Ade *et al.*, “Planck 2015 results. XIII. Cosmological parameters,” *Astron. Astrophys.*, vol. 594, p. A13, 2016.
- [6] M. Tegmark *et al.*, “Cosmological parameters from SDSS and WMAP,” *Phys. Rev. D*, vol. 69, p. 103501, 2004.
- [7] D. J. Eisenstein *et al.*, “Detection of the Baryon Acoustic Peak in the Large-Scale Correlation Function of SDSS Luminous Red Galaxies,” *Astrophys. J.*, vol. 633, pp. 560–574, 2005.
- [8] M. Tegmark *et al.*, “Cosmological Constraints from the SDSS Luminous Red Galaxies,” *Phys. Rev. D*, vol. 74, p. 123507, 2006.
- [9] S. Dodelson and L. Knox, “Dark energy and the CMB,” *Phys. Rev. Lett.*, vol. 84, p. 3523, 2000.
- [10] X.-m. Wang, M. Tegmark, and M. Zaldarriaga, “Is cosmology consistent?,” *Phys. Rev. D*, vol. 65, p. 123001, 2002.
- [11] U. Seljak, A. Slosar, and P. McDonald, “Cosmological parameters from combining the Lyman-alpha forest with CMB, galaxy clustering and SN constraints,” *JCAP*, vol. 10, p. 014, 2006.
- [12] M. Tegmark *et al.*, “Towards a refined cosmic concordance model: Joint 11 parameter constraints from CMB and large scale structure,” *Phys. Rev. D*, vol. 63, p. 043007, 2001.
- [13] W. Handley, “Curvature tension: evidence for a closed universe,” *Phys. Rev. D*, vol. 103, no. 4, p. L041301, 2021.
- [14] E. Di Valentino *et al.*, “Planck evidence for a closed Universe and a possible crisis for cosmology,” *Nature Astron.*, vol. 4, no. 2, pp. 196–203, 2019.
- [15] Y. Zhang and W. Fang, “Geometrical constraints on curvature from galaxy-lensing cross-correlations,” *Phys. Rev. D*, vol. 103, no. 4, p. 043539, 2021.
- [16] R. Arjona and S. Nesseris, “Novel null tests for the spatial curvature and homogeneity of the Universe and their machine learning reconstructions,” *Phys. Rev. D*, vol. 103, no. 10, p. 103539, 2021.
- [17] J. E. Gonzalez *et al.*, “Testing the consistency between cosmological data: the impact of spatial curvature and the dark energy EoS,” *JCAP*, vol. 11, no. 11, p. 060, 2021.
- [18] J. F. Jesus *et al.*, “Kinematic Constraints on Spatial Curvature from Supernovae Ia and Cosmic Chronometers,” *Mon. Not. Roy. Astron. Soc.*, vol. 500, no. 2, pp. 2227–2235, 2020.
- [19] G. G. Luciano, “Cosmic evolution and thermal stability of Barrow holographic dark energy in a nonflat Friedmann-Robertson-Walker Universe,” *Phys. Rev. D*, vol. 106, no. 8, p. 083530, 2022.

- [20] Y.-J. Wang *et al.*, “Cosmological model-independent measurement of cosmic curvature using distance sum rule with the help of gravitational waves,” *Mon. Not. Roy. Astron. Soc.*, vol. 516, no. 4, pp. 5187–5195, 2022.
- [21] J.-Z. Qi *et al.*, “Strongly lensed type Ia supernovae as a precise late-Universe probe of measuring the Hubble constant and cosmic curvature,” *Phys. Rev. D*, vol. 106, no. 2, p. 023520, 2022.
- [22] L. Amendola, M. Marinucci, and M. Quartin, “Spatial curvature with the Alcock-Paczynski effect,” 4 2024.
- [23] D. Andriot, D. Tsimpis, and T. Wrase, “Accelerated expansion of an open universe and string theory realizations,” *Phys. Rev. D*, vol. 108, no. 12, p. 123515, 2023.
- [24] D. Andriot, S. Parameswaran, D. Tsimpis, T. Wrase, and I. Zavala, “Exponential Quintessence: curved, steep and stringy?,” 5 2024.
- [25] S. Bhattacharya, G. Borghetto, A. Malhotra, S. Parameswaran, G. Tasinato, and I. Zavala, “Cosmological constraints on curved quintessence,” 5 2024.
- [26] N. Aghanim *et al.*, “Planck 2018 results. VI. Cosmological parameters,” *Astron. Astrophys.*, vol. 641, p. A6, 2020. [Erratum: *Astron. Astrophys.* 652, C4 (2021)].
- [27] S. Alam *et al.*, “The clustering of galaxies in the completed SDSS-III Baryon Oscillation Spectroscopic Survey: cosmological analysis of the DR12 galaxy sample,” *Monthly Notices of the Royal Astronomical Society*, vol. 470, pp. 2617–2652, 03 2017.
- [28] S. Alam *et al.*, “Completed SDSS-IV extended Baryon Oscillation Spectroscopic Survey: Cosmological implications from two decades of spectroscopic surveys at the Apache Point Observatory,” *Phys. Rev. D*, vol. 103, no. 8, p. 083533, 2021.
- [29] A. Glanville, C. Howlett, and T. M. Davis, “Full-shape galaxy power spectra and the curvature tension,” *Mon. Not. Roy. Astron. Soc.*, vol. 517, no. 2, pp. 3087–3100, 2022.
- [30] S. Vagnozzi, E. Di Valentino, S. Gariazzo, A. Melchiorri, O. Mena, and J. Silk, “The galaxy power spectrum take on spatial curvature and cosmic concordance,” *Phys. Dark Univ.*, vol. 33, p. 100851, 2021.
- [31] J.-Z. Qi, P. Meng, J.-F. Zhang, and X. Zhang, “Model-independent measurement of cosmic curvature with the latest $H(z)$ and SNe Ia data: A comprehensive investigation,” *Phys. Rev. D*, vol. 108, no. 6, p. 063522, 2023.
- [32] S. Anselmi, M. F. Carney, J. T. Giblin, S. Kumar, J. B. Mertens, M. O’Dwyer, G. D. Starkman, and C. Tian, “What is flat Λ CDM, and may we choose it?,” *JCAP*, vol. 02, p. 049, 2023.
- [33] J. Dossett and M. Ishak, “Spatial Curvature and Cosmological Tests of General Relativity,” *Phys. Rev. D*, vol. 86, p. 103008, 2012.
- [34] W. Yang, W. Giarè, S. Pan, E. Di Valentino, A. Melchiorri, and J. Silk, “Revealing the effects of curvature on the cosmological models,” *Phys. Rev. D*, vol. 107, no. 6, p. 063509, 2023.
- [35] E. Di Valentino, A. Melchiorri, and J. Silk, “Investigating Cosmic Discordance,” *Astrophys. J. Lett.*, vol. 908, no. 1, p. L9, 2021.
- [36] J. de Cruz Perez, C.-G. Park, and B. Ratra, “Updated observational constraints on spatially-flat and non-flat Λ CDM and XCDM cosmological models,” *arXiv: 2404.19194*, 2024.

- [37] W. Yang, S. Pan, E. Di Valentino, O. Mena, and A. Melchiorri, “2021- H_0 odyssey: closed, phantom and interacting dark energy cosmologies,” *JCAP*, vol. 10, p. 008, 2021.
- [38] M. Benetti, H. Borges, C. Pigozzo, S. Carneiro, and J. Alcaniz, “Dark sector interactions and the curvature of the universe in light of Planck’s 2018 data,” *JCAP*, vol. 08, p. 014, 2021.
- [39] A. G. Adame *et al.*, “DESI 2024 VI: Cosmological Constraints from the Measurements of Baryon Acoustic Oscillations,” *FERMILAB-PUB-24-0154-PPD*, arXiv:2404.03002.
- [40] T. Liu, S. Cao, X. Li, H. Zheng, Y. Liu, W. Guo, and C. Zheng, “Revising the Hubble constant, spatial curvature and dark energy dynamics with the latest observations of quasars,” *Astron. Astrophys.*, vol. 668, p. A51, 2022.
- [41] K. Bolejko, “Emerging spatial curvature can resolve the tension between high-redshift CMB and low-redshift distance ladder measurements of the Hubble constant,” *Phys. Rev. D*, vol. 97, no. 10, p. 103529, 2018.
- [42] A. G. Riess *et al.*, “A comprehensive measurement of the local value of the hubble constant with 1 km/s/mpc uncertainty from the hubble space telescope and the sh0es team,” *Astrophys. J. Lett.*, vol. 934, no. 1, p. L7, 2022.
- [43] C. Heymans *et al.*, “KiDS-1000 Cosmology: Multi-probe weak gravitational lensing and spectroscopic galaxy clustering constraints,” *Astron. Astrophys.*, vol. 646, p. A140, 2021.
- [44] L. F. Secco *et al.*, “Dark Energy Survey Year 3 results: Cosmology from cosmic shear and robustness to modeling uncertainty,” *Phys. Rev. D*, vol. 105, no. 2, p. 023515, 2022.
- [45] T. M. C. Abbott *et al.*, “Dark Energy Survey Year 3 results: Constraints on extensions to Λ CDM with weak lensing and galaxy clustering,” *Phys. Rev. D*, vol. 107, no. 8, p. 083504, 2023.
- [46] E. Di Valentino *et al.*, “Cosmology intertwined iii: $f\sigma_8$ and s_8 ,” *Astroparticle Physics*, vol. 131, p. 102604, 2021.
- [47] W. Yang, S. Pan, E. Di Valentino, R. C. Nunes, S. Vagnozzi, and D. F. Mota, “Tale of stable interacting dark energy, observational signatures, and the H_0 tension,” *JCAP*, vol. 09, p. 019, 2018.
- [48] B. Wang, E. Abdalla, F. Atrio-Barandela, and D. Pavón, “Dark matter and dark energy interactions: theoretical challenges, cosmological implications and observational signatures,” *Reports on Progress in Physics*, vol. 79, p. 096901, aug 2016.
- [49] S. A. Adil, O. Akarsu, E. Di Valentino, R. C. Nunes, E. Özlüker, A. A. Sen, and E. Specogna, “Omnipotent dark energy: A phenomenological answer to the Hubble tension,” *Phys. Rev. D*, vol. 109, no. 2, p. 023527, 2024.
- [50] L. Verde, T. Treu, and A. G. Riess, “Tensions between the Early and the Late Universe,” *Nature Astron.*, vol. 3, p. 891, 7 2019.
- [51] J. Evslin, A. A. Sen, and Ruchika, “Price of shifting the Hubble constant,” *Phys. Rev. D*, vol. 97, no. 10, p. 103511, 2018.
- [52] W. Yang, A. Mukherjee, E. Di Valentino, and S. Pan, “Interacting dark energy with time varying equation of state and the H_0 tension,” *Phys. Rev. D*, vol. 98, no. 12, p. 123527, 2018.
- [53] T. Karwal, M. Raveri, B. Jain, J. Khoury, and M. Trodden, “Chameleon early dark energy and the Hubble tension,” *Phys. Rev. D*, vol. 105, no. 6, p. 063535, 2022.

- [54] K. Freese and M. W. Winkler, “Chain early dark energy: A Proposal for solving the Hubble tension and explaining today’s dark energy,” *Phys. Rev. D*, vol. 104, no. 8, p. 083533, 2021.
- [55] J. S. Cruz, F. Niedermann, and M. S. Sloth, “A grounded perspective on new early dark energy using ACT, SPT, and BICEP/Keck,” *JCAP*, vol. 02, p. 041, 2023.
- [56] G. Franco Abellán, R. Murgia, and V. Poulin, “Linear cosmological constraints on two-body decaying dark matter scenarios and the S8 tension,” *Phys. Rev. D*, vol. 104, no. 12, p. 123533, 2021.
- [57] F. Okamoto, T. Sekiguchi, and T. Takahashi, “ H_0 tension without CMB data: Beyond the Λ CDM,” *Phys. Rev. D*, vol. 104, no. 2, p. 023523, 2021.
- [58] A. Banerjee, H. Cai, L. Heisenberg, E. O. Colgáin, M. M. Sheikh-Jabbari, and T. Yang, “Hubble sinks in the low-redshift swampland,” *Phys. Rev. D*, vol. 103, no. 8, p. L081305, 2021.
- [59] B.-H. Lee, W. Lee, E. O. Colgáin, M. M. Sheikh-Jabbari, and S. Thakur, “Is local H_0 at odds with dark energy EFT?,” *JCAP*, vol. 04, no. 04, p. 004, 2022.
- [60] D. Chowdhury, G. Tasinato, and I. Zavala, “Dark energy, D-branes, and Pulsar Timing Arrays,” 7 2023.
- [61] G. Montani, M. De Angelis, F. Bombacigno, and N. Carlevaro, “Metric $f(R)$ gravity with dynamical dark energy as a paradigm for the Hubble Tension,” 6 2023.
- [62] J. C. N. de Araujo *et al.*, “Minimal theory of massive gravity in the light of CMB data and the S8 tension,” *Phys. Rev. D*, vol. 104, no. 10, p. 104057, 2021.
- [63] L. Knox and M. Millea, “Hubble constant hunter’s guide,” *Phys. Rev. D*, vol. 101, no. 4, p. 043533, 2020.
- [64] E. Di Valentino *et al.*, “Snowmass2021 - Letter of interest cosmology intertwined II: The hubble constant tension,” *Astropart. Phys.*, vol. 131, p. 102605, 2021.
- [65] E. Di Valentino, O. Mena, S. Pan, L. Visinelli, W. Yang, A. Melchiorri, D. F. Mota, A. G. Riess, and J. Silk, “In the realm of the Hubble tension—a review of solutions,” *Class. Quant. Grav.*, vol. 38, no. 15, p. 153001, 2021.
- [66] A. A. Sen, S. A. Adil, and S. Sen, “Do cosmological observations allow a negative Λ ?,” *Mon. Not. Roy. Astron. Soc.*, vol. 518, no. 1, pp. 1098–1105, 2022.
- [67] L. A. Escamilla, O. Akarsu, E. Di Valentino, and J. A. Vazquez, “Model-independent reconstruction of the Interacting Dark Energy Kernel: Binned and Gaussian process,” 2023.
- [68] M. Rezaei and J. Sola Peracaula, “Running vacuum versus holographic dark energy: a cosmographic comparison,” *Eur. Phys. J. C*, vol. 82, no. 8, p. 765, 2022.
- [69] M. Rezaei, J. Solà Peracaula, and M. Malekjani, “Cosmographic approach to Running Vacuum dark energy models: new constraints using BAOs and Hubble diagrams at higher redshifts,” *Mon. Not. Roy. Astron. Soc.*, vol. 509, no. 2, pp. 2593–2608, 2021.
- [70] T. Patil and S. Panda, “Coupled scalar field cosmology with effects of curvature,” *Eur. Phys. J. Plus*, vol. 138, no. 7, p. 583, 2023.
- [71] T. Patil, S. Panda, M. Sharma, and Ruchika, “Dynamics of interacting scalar field model in the realm of chiral cosmology,” *Eur. Phys. J. C*, vol. 83, no. 2, p. 131, 2023.

- [72] M. Rezaei, M. Malekjani, and J. Sola, “Can dark energy be expressed as a power series of the Hubble parameter?,” *Phys. Rev. D*, vol. 100, no. 2, p. 023539, 2019.
- [73] B. J. Barros, L. Amendola, T. Barreiro, and N. J. Nunes, “Coupled quintessence with a Λ CDM background: removing the σ_8 tension,” *JCAP*, vol. 01, p. 007, 2019.
- [74] L. Amendola, “Coupled quintessence,” *Phys. Rev. D*, vol. 62, p. 043511, Jul 2000.
- [75] E. Abdalla *et al.*, “Cosmology intertwined: A review of the particle physics, astrophysics, and cosmology associated with the cosmological tensions and anomalies,” *JHEAp*, vol. 34, pp. 49–211, 2022.
- [76] T. Patil, Ruchika, and S. Panda, “Coupled Quintessence scalar field model in light of observational datasets,” *Journal of Cosmology and Astroparticle Physics*, vol. 2024, no. 05, p. 033, 2024.
- [77] M. Lucca and D. C. Hooper, “Shedding light on dark matter-dark energy interactions,” *Phys. Rev. D*, vol. 102, no. 12, p. 123502, 2020.
- [78] L.-Y. Gao, S.-S. Xue, and X. Zhang, “Dark energy and matter interacting scenario to relieve H_0 and S_8 tensions*,” *Chin. Phys. C*, vol. 48, no. 5, p. 051001, 2024.
- [79] S. Kumar and R. C. Nunes, “Echo of interactions in the dark sector,” *Phys. Rev. D*, vol. 96, no. 10, p. 103511, 2017.
- [80] S. Gariazzo, E. Di Valentino, O. Mena, and R. C. Nunes, “Late-time interacting cosmologies and the Hubble constant tension,” *Phys. Rev. D*, vol. 106, no. 2, p. 023530, 2022.
- [81] V. Salvatelli, N. Said, M. Bruni, A. Melchiorri, and D. Wands, “Indications of a late-time interaction in the dark sector,” *Phys. Rev. Lett.*, vol. 113, no. 18, p. 181301, 2014.
- [82] M. G. Richarte and L. Xu, “Exploring a new interaction between dark matter and dark energy using the growth rate of structure,” 6 2015.
- [83] R. C. Nunes, S. Pan, and E. N. Saridakis, “New constraints on interacting dark energy from cosmic chronometers,” *Phys. Rev. D*, vol. 94, no. 2, p. 023508, 2016.
- [84] E. Di Valentino, A. Melchiorri, O. Mena, S. Pan, and W. Yang, “Interacting Dark Energy in a closed universe,” *Mon. Not. Roy. Astron. Soc.*, vol. 502, no. 1, pp. L23–L28, 2021.
- [85] A. de Mattia *et al.*, “The Completed SDSS-IV extended Baryon Oscillation Spectroscopic Survey: measurement of the BAO and growth rate of structure of the emission line galaxy sample from the anisotropic power spectrum between redshift 0.6 and 1.1,” *Mon. Not. Roy. Astron. Soc.*, vol. 501, no. 4, pp. 5616–5645, 2021.
- [86] A. Raichoor *et al.*, “The completed SDSS-IV extended Baryon Oscillation Spectroscopic Survey: Large-scale Structure Catalogues and Measurement of the isotropic BAO between redshift 0.6 and 1.1 for the Emission Line Galaxy Sample,” *Mon. Not. Roy. Astron. Soc.*, vol. 500, no. 3, pp. 3254–3274, 2020.
- [87] J. E. Bautista *et al.*, “The Completed SDSS-IV extended Baryon Oscillation Spectroscopic Survey: measurement of the BAO and growth rate of structure of the luminous red galaxy sample from the anisotropic correlation function between redshifts 0.6 and 1,” *Mon. Not. Roy. Astron. Soc.*, vol. 500, no. 1, pp. 736–762, 2020.

- [88] J. Hou *et al.*, “The Completed SDSS-IV extended Baryon Oscillation Spectroscopic Survey: BAO and RSD measurements from anisotropic clustering analysis of the Quasar Sample in configuration space between redshift 0.8 and 2.2,” *Mon. Not. Roy. Astron. Soc.*, vol. 500, no. 1, pp. 1201–1221, 2020.
- [89] V. Bonvin *et al.*, “H0LiCOW – V. New COSMOGRAIL time delays of HE 0435–1223: H_0 to 3.8 per cent precision from strong lensing in a flat Λ CDM model,” *Mon. Not. Roy. Astron. Soc.*, vol. 465, no. 4, pp. 4914–4930, 2017.
- [90] L. Amendola and D. Tocchini-Valentini, “Baryon bias and structure formation in an accelerating universe,” *Phys. Rev. D*, vol. 66, p. 043528, 2002.
- [91] T. Damour and C. Gundlach, “Nucleosynthesis constraints on an extended Jordan-Brans-Dicke theory,” *Phys. Rev. D*, vol. 43, pp. 3873–3877, Jun 1991.
- [92] R. R. Caldwell and E. V. Linder, “The Limits of quintessence,” *Phys. Rev. Lett.*, vol. 95, p. 141301, 2005.
- [93] L. Chen, Q.-G. Huang, and K. Wang, “Distance Priors from Planck Final Release,” *JCAP*, vol. 02, p. 028, 2019.
- [94] P. A. R. Ade *et al.*, “Planck 2015 results. XIV. Dark energy and modified gravity,” *Astron. Astrophys.*, vol. 594, p. A14, 2016.
- [95] Z. Zhai, C.-G. Park, Y. Wang, and B. Ratra, “CMB distance priors revisited: effects of dark energy dynamics, spatial curvature, primordial power spectrum, and neutrino parameters,” *JCAP*, vol. 07, p. 009, 2020.
- [96] M. Rezaei, M. Malekjani, and J. Sola, “Can dark energy be expressed as a power series of the Hubble parameter?,” *Phys. Rev. D*, vol. 100, no. 2, p. 023539, 2019.
- [97] R. Arjona, W. Cardona, and S. Nesseris, “Designing Horndeski and the effective fluid approach,” *Phys. Rev. D*, vol. 100, no. 6, p. 063526, 2019.
- [98] Z. Zhai and Y. Wang, “Robust and model-independent cosmological constraints from distance measurements,” *JCAP*, vol. 07, p. 005, 2019.
- [99] R. Lazkoz, R. Maartens, and E. Majerotto, “Observational constraints on phantom-like braneworld cosmologies,” *Phys. Rev. D*, vol. 74, p. 083510, 2006.
- [100] P. S. Corasaniti and A. Melchiorri, “Testing cosmology with cosmic sound waves,” *Phys. Rev. D*, vol. 77, p. 103507, 2008.
- [101] O. Elgaroy and T. Multamaki, “On using the CMB shift parameter in tests of models of dark energy,” *Astron. Astrophys.*, vol. 471, p. 65, 2007.
- [102] F. Beutler *et al.*, “The 6df galaxy survey: baryon acoustic oscillations and the local Hubble constant,” *Monthly Notices of the Royal Astronomical Society*, vol. 416, pp. 3017–3032, Jul 2011.
- [103] A. J. Ross, L. Samushia, C. Howlett, W. J. Percival, A. Burden, and M. Manera, “The clustering of the SDSS DR7 main Galaxy sample – I. A 4 per cent distance measure at $z = 0.15$,” *Mon. Not. Roy. Astron. Soc.*, vol. 449, no. 1, pp. 835–847, 2015.
- [104] M. Ata *et al.*, “The clustering of the SDSS-IV extended Baryon Oscillation Spectroscopic Survey DR14 quasar sample: first measurement of baryon acoustic oscillations between redshift 0.8 and 2.2,” *Mon. Not. Roy. Astron. Soc.*, vol. 473, no. 4, pp. 4773–4794, 2018.

- [105] H. du Mas des Bourboux *et al.*, “Baryon acoustic oscillations from the complete SDSS-III Ly α -quasar cross-correlation function at $z = 2.4$,” *Astron. Astrophys.*, vol. 608, p. A130, 2017.
- [106] S. Alam *et al.*, “The clustering of galaxies in the completed SDSS-III Baryon Oscillation Spectroscopic Survey: cosmological analysis of the DR12 galaxy sample,” *Mon. Not. Roy. Astron. Soc.*, vol. 470, no. 3, pp. 2617–2652, 2017.
- [107] M. Moresco, A. Cimatti, R. Jimenez, and et. al, “Improved constraints on the expansion rate of the universe up to $z = 1.1$ from the spectroscopic evolution of cosmic chronometers,” *Journal of Cosmology and Astroparticle Physics*, vol. 2012, no. 08, p. 006–006, 2012.
- [108] M. Moresco, “Raising the bar: new constraints on the Hubble parameter with cosmic chronometers at $z \sim 2$,” *Mon. Not. Roy. Astron. Soc.*, vol. 450, no. 1, pp. L16–L20, 2015.
- [109] M. Moresco, L. Pozzetti, A. Cimatti, R. Jimenez, C. Maraston, L. Verde, D. Thomas, A. Citro, R. Tojeiro, and D. Wilkinson, “A 6% measurement of the Hubble parameter at $z \sim 0.45$: direct evidence of the epoch of cosmic re-acceleration,” *JCAP*, vol. 05, p. 014, 2016.
- [110] D. Scolnic *et al.*, “The Pantheon+ Analysis: The Full Data Set and Light-curve Release,” *Astrophys. J.*, vol. 938, no. 2, p. 113, 2022.
- [111] D. Brout *et al.*, “The Pantheon+ Analysis: Cosmological Constraints,” *Astrophys. J.*, vol. 938, no. 2, p. 110, 2022.
- [112] M. J. Reid, J. A. Braatz, J. J. Condon, L. J. Greenhill, C. Henkel, and K. Y. Lo, “The megamaser cosmology project. i. very long baseline interferometric observations of ugc 3789,” *The Astrophysical Journal*, vol. 695, p. 287, mar 2009.
- [113] J. A. Braatz, M. J. Reid, E. M. L. Humphreys, C. Henkel, J. J. Condon, and K. Lo, “The megamaser cosmology project. ii. the angular-diameter distance to ugc 3789,” *The Astrophysical Journal*, vol. 718, p. 657, jul 2010.
- [114] M. J. Reid, J. A. Braatz, J. J. Condon, K. Y. Lo, C. Y. Kuo, C. M. V. Impellizzeri, and C. Henkel, “The megamaser cosmology project. iv. a direct measurement of the hubble constant from ugc 3789,” *The Astrophysical Journal*, vol. 767, p. 154, apr 2013.
- [115] C. Y. Kuo, J. A. Braatz, M. J. Reid, K. Y. Lo, J. J. Condon, C. M. V. Impellizzeri, and C. Henkel, “The megamaser cosmology project. v. an angular-diameter distance to ngc 6264 at 140 mpc,” *The Astrophysical Journal*, vol. 767, p. 155, apr 2013.
- [116] F. Gao, J. A. Braatz, M. J. Reid, K. Y. Lo, J. J. Condon, C. Henkel, C. Y. Kuo, C. M. V. Impellizzeri, D. W. Pesce, and W. Zhao, “The megamaser cosmology project. viii. a geometric distance to ngc 5765b,” *The Astrophysical Journal*, vol. 817, p. 128, jan 2016.
- [117] S. Basilakos, S. Nesseris, and L. Perivolaropoulos, “Observational constraints on viable $f(R)$ parametrizations with geometrical and dynamical probes,” *Phys. Rev. D*, vol. 87, no. 12, p. 123529, 2013.
- [118] D. Foreman-Mackey, D. W. Hogg, D. Lang, and J. Goodman, “emcee: The mcmc hammer,” *Publications of the Astronomical Society of the Pacific*, vol. 125, p. 306, feb 2013.
- [119] T. M. C. Abbott *et al.*, “Dark Energy Survey Year 3 results: Cosmological constraints from galaxy clustering and weak lensing,” *Phys. Rev. D*, vol. 105, no. 2, p. 023520, 2022.
- [120] L. Amendola *et al.*, “Cosmology and fundamental physics with the Euclid satellite,” *Living Rev. Rel.*, vol. 21, no. 1, p. 2, 2018.

- [121] D. J. Schlegel *et al.*, “A Spectroscopic Road Map for Cosmic Frontier: DESI, DESI-II, Stage-5,” arXiv:2209.03585.
- [122] L. Perenon, S. Ilíc, R. Maartens, and A. de la Cruz-Dombriz, “Improvements in cosmological constraints from breaking growth degeneracy,” *Astron. Astrophys.*, vol. 642, p. A116, 2020.
- [123] A. Orsi *et al.*, “Probing dark energy with future redshift surveys: a comparison of emission line and broad-band selection in the near-infrared,” *Mon. Not. Roy. Astron. Soc.*, vol. 405, pp. 1006–1024, 06 2010.
- [124] V. Yankelevich and C. Porciani, “Cosmological information in the redshift-space bispectrum,” *Mon. Not. Roy. Astron. Soc.*, vol. 483, no. 2, pp. 2078–2099, 2019.